Validated E-field Measurement Setup for SAR Estimation in Human Phantom Model

Conference Paper · March 2023

DOI: 10.23919/EuCAP57121.2023.10133159

8 authors, including:

Manuel Ricardo Pérez Cerquera
Pontificia Universidad Javeriana
46 PUBLICATIONS **352** CITATIONS
SEE PROFILE

Robert Urbina
Pontificia Universidad Javeriana
10 PUBLICATIONS **7** CITATIONS
SEE PROFILE

Andres Gallego
National University of Colombia
13 PUBLICATIONS **18** CITATIONS
SEE PROFILE

Arturo Fajardo
Pontificia Universidad Javeriana
55 PUBLICATIONS **183** CITATIONS
SEE PROFILE

Validated E-field Measurement Setup for SAR Estimation in Human Phantom Model

M. Pérez*, R. Urbina*, C. Durán*, G. Martínez†, A. Gallego†, A. Fajardo *, C.I. Páez-Rueda *, J.L. Araque †
*Pontificia Universidad Javeriana, Dept. of Electronics Engineering, Bogotá D.C. 110231, Colombia
†Universidad Nacional de Colombia, Ciudad Universitaria, Bogotá D.C. 111321, Colombia
Corresponding author: manuel.perez@javeriana.edu.co

***Abstract*—This paper describes the validation of an experimental E-field and Specific Absorption Rate (SAR) measurement setup for RF exposure assessment in a human flat phantom model. The requirements of standards related to RF dosimetry were taken into account for the integration of the experimental setup. From the various test cases tackled, we present results on the accuracy and precision of the E-field probe tracking system, and the comparison of measured E-field/SAR hot maps with simulations, which presented good agreement.**

***Index Terms*—RF dosymetry, non-ionizing radiation, RF dosimetry, RF/microwave exposure assessment, SAR measurement systems, specific absorption rate (SAR) measurements.**

I. Introduction

According to the International Commission on Nonionizing Radiation Protection (ICNIRP), exposure to electromagnetic fields with frequencies above 100 kHz can cause significant energy absorption within the human body, resulting in an increase in body temperature and highly non-uniform deposition and distribution of energy within the body, which must be evaluated through measurement and dosimetric calculations [1]. There is currently a longstanding concern about the health consequences of uncontrolled exposure to RF radiation [2].

Although the only proven effect of non-ionizing radiation is heating of exposed tissues, there have been warnings about the possible carcinogenic risks. Based on the review of the existing literature about epidemiological studies in humans and animals, the International Agency for Research on Cancer (IARC) and the World Health Organization (WHO) classified Electromagnetic Field (EMF) radiation as a possible human carcinogen (Group 2B) [3]. These studies revealed that the risk of developing brain tumors (gliomas) and vestibular Schwannomas increased in people who used mobile phones more frequently, particularly in people who used mobile phones on the same side of the head where the tumor developed [4].

Another method for estimating dosimetrical RF radiation metrics in the human body, such as electric field intensity and Specific Absorption Rate (SAR), is to use 3D computational models that include body parts with dielectric properties as well as radiation sources [5]. Similarly, other works validate computational models using phantom models and mobile terminals set ups in anechoic chambers [6], [7]. The majority of studies reported using this phantom models adhere to the IEEE 1528 measurement standard which gives the guidelines to determine the peak SAR [8]. The SAR measurement is proportional to the increase in temperature at a specific point within the tissue.

Dosimetric assessment methodologies with human phantom models have been already proposed. As for instance, the work in [6] proposes a biotic tissue-equivalent solid human head phantom model for experimental estimation of the electromagnetic energy field induced in the human head. The proposed phantom includes a brain and skull-equivalent model for performing SAR estimation in the human head which is then validated using a thermographic method. Despite the obtained results of SAR estimation inside canonical and anthropomorphic head phantom models through the thermographic approach are very consistent, the authors conclude that this approach has limitations when obtaining 3D SAR distributions for computing the 1- or 10-g average SAR, and therefore it is not suitable to test real RF devices. The work in [7] presents a characterization study of the SAR inside a child head phantom due to the use of mobile phones. The motivation of the study in child heads is because the size difference regarding an adult head presented in previous studies [9]. Therefore, the study is centered in SAR measurements inside child and adult head phantoms for several cellular phones commercially available. SAR distribution results are presented in flat and biotic phantoms with several types of phones operating in the frequency band of 800 MHz. The study concludes that the position of the peak SAR and SAR distribution vary due to the antenna position. Despite, the results are clear and the research hypothesis is proven, details about the experimental setup are missing.

More recently we have already proposed a low-cost system for electromagnetic SAR evaluation in an anthropomorphic human phantom [10], [11], [12]. The previous work has been focused on the construction process of the developed in-house tracking system with web-cameras, the manufacturing of the shell for the human phantom, and the preparation of tissue-emulating liquid. However, first results were only limited to obtain the field distribution of a horn-antenna with low resolution, which were not validated through simulation.

This paper is based on the previous experimental setup but in this work we have extended the description of each subsystem of the proposed SAR estimation system. Additionally, validation of Electric field distribution results are also presented through simulation in Ansys Electronics Desktop and accuracy specifications are also given for the optic tracking system.

This paper is structured as follows. Section II presents in detail the subsystems that integrate the experimental electric field and SAR measurement setup. Section III presents the setup validation test and the analysis results. Finally, section IV concludes this work.

II. Experimental E-Field Measurement Setup

The experimental setup was configured following the guides given in the standards [8], [13], [14]. In the standards, reproducible and repeatable protocols and test procedures are specified for the measurement of the peak spatial average SAR induced inside simplified models of the head and the body by radio-frequency transmitting devices. On one hand, the standards in [8], [13] present procedures that apply to handheld and body-worn wireless communication devices intended to be used for personal services with single or multiple transmitters or antennas at distances up to 200 mm from human head or body, operating in the frequency band between 4 MHz to 10 GHz. On the other hand, the standard [14] addresses the evaluation of RF field strength or SAR levels in the vicinity of non-broadcast RF radiocommunication sources intentionally radiating for the purpose of evaluation human exposure, in the frequency range of 300 MHz to 6 GHz.

Terms and definitions are given in the standards, one of the most important is the Specific Absorption Rate (SAR) which is a measure of the rate at which energy is absorbed by the human body when exposed to a radio frequency electromagnetic field. In other words SAR is the the time derivative (rate) of the incremental energy ($dW\,[W]$) absorbed by (dissipated in) an incremental mass ($dm\,[kg]$) contained in a volume element ($dV\,[m^3]$) of a given mass density ($\rho\,[kg/m^3]$), as expressed in the equation (1).

$$SAR = \frac{d}{dt}\left(\frac{dW}{dm}\right) = \frac{d}{dt}\left(\frac{dW}{\rho\, dV}\right)\left[\frac{W}{kg}\right] \tag{1}$$

SAR is related to the E-field at a point by the first equality in equation (2), and it can also be determined by the rate of temperature increase by the second equality in equation (2).

$$SAR = \frac{\sigma E^2}{\rho} = c_h \frac{\partial T}{\partial t}\bigg|_{t=0} \tag{2}$$

where E is the RMS value of the electric field strength in the tissue-equivalent medium in V/m, σ is the electrical conductivity in S/m, c_h the heat capacity in J/K and $\partial T/\partial t|_{t=0}$ is the initial time derivative of temperature in k/s, all values of the tissue-equivalent medium.

In addition, standards also give the general requirements for the E-field probe, the phantom selection and the tissue-equivalent medium. E-field probe requirements are to be electrically small compared with the wavelength in the tissue-equivalent liquid, be isotropic, exhibit a linear response to the square of the incident E-field strength, and shall be transparent (nonperturbing) to the measured field [8]. In terms of the phantom selection, a flat-boxed-shaped whole-body phantom shall be used with lateral dimensions of 1.54 m $\times$ 0.339 m and shell thickness up to 3 mm [14]. Additionally, phantom shell shall be made of low-loss low-permittivity material, having loss tangent $tan\,\delta \leq 0.05$ and relative permittivity $\varepsilon_r' \leq 5$ for frequencies under 3 GHz and $3 \geq \varepsilon_r' \leq 5$, for frequencies above 3GHz [13]. Finally, the target dielectric properties of the tissue-equivalent medium to fill the phantom are specified in [13] for discrete frequencies ranging between 4 MHz and 10 GHz, where linear interpolation are suggested for other frequencies within the range. Example recipes for preparing tissue-equivalent media designed to produce the dielectric properties in the operating frequency range are provided in [13] and procedures and conditions for characterization of tissue-equivalent liquid dielectric properties are given in [8], where room temperature (18°C to 25°C) is advised for simulating the same parameters at body temperature (37°C) and coaxial probe is one of the methods for the liquid characterization. Other important requirements are: i) The measurement should be performed at the highest output power level. Alternatively, the measurement may be performed at a known lower power level and the result scaled to the highest power level numerically. ii) To determine the maximum SAR, the evaluation shall be performed with the antenna, or the side of the device where the antenna is located, facing the phantom. The antenna or device shall be positioned so as to obtain the highest possible SAR. In addition, during the measurements the centre of the antenna shall be placed below the centre of the phantom in order to avoid that an antenna element is positioned close to an edge of the phantom.iii) To establish the compliance boundary, testing shall be performed at different separation distances between 5 mm and up to 1000 mm from the tissue simulating liquid to determine the compliance distance.

By considering the aforementioned requirements and considerations, we have proposed the measurement setup shown in Fig.1. The setup is integrated by 5 systems: A) The tracking system, which is used for localization of the E-Field probe in the tissue-equivalent liquid inside the phantom during the measurement process. For this, a high-performance optical tracking system were integrated. B) The dielectric properties measurement system, which is part of the procedure to characterize the dielectric properties of the tissue-equivalent liquid. For this, a coaxial probe method was used. C) The Electric field measurement system, where a flat body phantom filled with the liquid and a E-field probe were employed. D) The radio-frequency signal generation system, where a vector signal generator was used which delivers a power up to 30 dBm and a frequency up to 20 GHz. In addition, a horn antenna was used for validation and test. Finally, E) a data post processing system where the tracked position of the probe and the E-field measurement are associated for obtaining 2D heat maps. In the following, the description of the system are presented in more detail.

A. Tracking system

OptiTrack™ offers high-performance optical tracking at the most affordable prices in the industry. This system uses

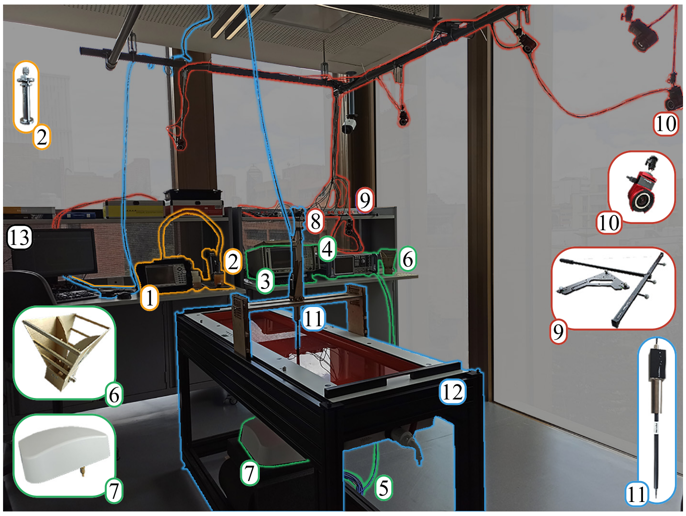

Fig. 1. Experimental setup: E-field measurement system Dielectric property measurement system Generation system Tracking system
1) Vector Analyzer ANRITSU MS2027C [15] 2) Probe DAK 3.5 [16] 3) Signal Analyzer LSA-132 4) Vector signal Generator SMW200A [17] 5) Wire CBL-25FT-SMSM+ 6) Horn Antenna SAS-571 [18] 7) Directional Panel Anenna PLTE7027M 8) Tracking markers 9) OptiTrack calibration 10) Camera Flex 13 11) Probe EF3DVX 12) Phantom BSP-A [19] 13) Computer.

markers and cameras (i.e., flex 13) to track the location of an object with an accuracy of less than 1 mm. The markers are attached to the probe that measures the electric field and it can thus be traced. Then, the probe is handily moved slowly through the different positions inside the Phantom. To reduce the vibrations of the movement, a structure is used to support and guide the trajectory (see Figure 1).

B. Dielectric property measurement system

To measure the dielectric properties of the tissue-equivalent liquid, the open-ended coaxial probe DAK 3.5 [16] and Vector Analyzer Network (VNA) MS2027C [15] were used. The VNA is configured to measure the magnitude and phase of the admittance. A one-port reflection calibration is performed at the plane of the probe in media with known or calculable reflection coefficients. Three standards are required for the calibration - typically a short circuit, air and a reference liquid. The complex relative permittivity $\varepsilon_r = \varepsilon_r' - j\sigma\omega\varepsilon_0$ is computed from the measured admittance. The detailed open-ended coaxial probe measurement procedure is detailed in [8]. The relative permittivity and conductivity are necessary to model the liquid in simulation and it also necessary for comparison with the standard. In addition, through the VNA the reflection coefficient of the horn antenna and the insertion losses of the feeding cable were obtained in order to know the isotropic radiation power of the signal generation system for scaling the feeding power in the simulation of the validation process.

C. E-field measurement system

In the experimental measurements, the human body is represented by the flat-phantom BSTP-A (Base Station Phantom Adult) [19]. This phantom is in accordance with the Base-Station Antenna Testing standards (i.e., IEC 62232 [14]). The Phantom is filled with the tissue-equivalent liquid HBBL600-10000V6 [20]. This liquid allows emulating the average dielectric properties of the human body tissues, with a specific absorption rate according to standards (i.e., IEC 62209[13], IEEE 1528 [8]). The liquid composition are made mainly of of de-ionizing water, oxidized mineral oil, diacetin, additives and salt. Suggested liquid recipes for achieving target dielectric properties are found in [13]. The Phantom is exposed to radiation from different antennas and the electric field intensity inside the liquid is measured under different conditions (e.g., different distance between the phantom and the antenna).

To measure the electric field, the probe EF3DV3 is used. This is a linear, isotropic E-Field probe for general near-field measurements which also allows measurement of SAR [21]. The probe was calibrated for the different frequency bands in which measurements are made.

D. Generation system

The radio-frequency wave radiated towards the phantom is produced by the vector signal generator SMW200A [17]. This generator has a wide range of frequencies (i.e., up to 67 GHz and for dual-path: up to 44 GHz), it delivers a power of up to 30 dBm and allows signal generation for all major digital communications standards. Furthermore, a signal analyzer LSA-132 is used to verify that the signal is correctly generated. The generator is connected to the antenna using a radio frequency wire CBL-25FT-SMSM+ with broadband coverage.

The antenna is located on the bottom of the phantom and pointing up. For the measurements, a double ridge guided horn antenna SAS-571 [18] was used for validation purposes since it has a commonly known radiation pattern, which allows reliable validation of experimental measurements with simulation.

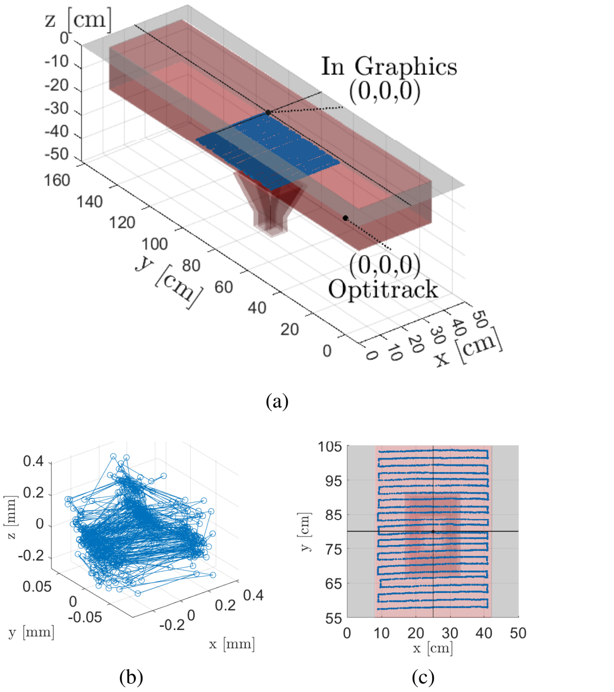

Fig. 2. Tracking with Optitrack system **a)** Positioning with respect to the phantom. **b)** One point accuracy. **b)** View of a tracked path.

E. Data post processing

Once the data are obtained, post-processing is performed. The measured electric field and the probe tracked position are associated using local time. By performing an interpolation, it is possible to reconstruct 2D hot maps and 3D volumes of the measured electric field and SAR in the phantom to identify hot-spots.

III. Test and Analysis Results

A. Tracking system

In order to associate E-field measurements to a position inside the phantom, accuracy and precision are necessary for the optical tracking system. To this end, two test were proposed, the first was to capture the position of the probe when it is moving on the supporting structure, in a horizontal plane as depicted in blue points in the perspective view of Fig. 2a and in a top view of Fig.2c. Therefore, position accuracy is tested regarding the boundary of the phantom digital twin that was generated using the measured corner points obtained with the optical system. Accuracy results show errors of less than 1 mm with respect to the real set-up. The second test was related to measure the precision of the tracking system. In this regard, the position of the probe was captured when it is static on the supporting structure. The variation of the tracked position of the probe is shown in Fig. 2b. The precision metric in this case were the estimated position standard deviation in the three axes $\sigma_x = 0.0213$ mm, $\sigma_y = 0.013$ mm and $\sigma_z = 0.0027mm$.

B. Dielectric property measurement system

Measurements of the dielectric properties of the tissue-equivalent liquid were performed with the calibrated coaxial probe of the DAK system. A total of approximately 80 L of liquid were necessary to fill the flat phantom and samples of 250 mL were taken to measure. The real and imaginary parts of the measured relative permittivity of the liquid in the frequency range between 200 MHz to 10 GHz are reported in Fig. 3. Different measures where taken in a time lapse of 1 year to analyze the liquid degradation. The room temperature of the experimental set-up was kept between 18°C and 23°C whereas the liquid temperature was between 19°C and 20°C. Measurements results were also compared with the dielectric properties suggested in the IEEE 1528 standard [8] and the calibrated curve provided by the liquid manufacturer.

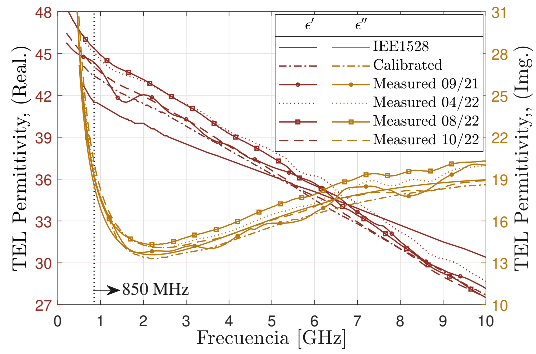

Fig. 3. Measured relative permittivity of the tissue-equivalent liquid (TEL).

C. Validation E-field measurement system

Validation were performed by simulation where the double ridge horn antenna, working at 850 MHz and separated from the phantom 10 cm, was modeled with the flat phantom shell filled with the tissue-equivalent liquid as it is shown in Fig. 4. In this scenario, the 2D hot map of the simulated and measured E-field and local SAR at 1 cm from the phantom shell were compared and reported in Fig. 5. Two main aspects were evaluated: First, the obtained radiation pattern where the two symmetrical radiation ridges with the nulls up and down in the y-axe are clearly identified in the results of both models and therefore consistency is reported. Second, the E-field peak values at the ridges where the difference is around 0.2 V/m and the 2D Root Mean Squared Error (RMSE) between measured and simulated patterns was 2.68 V/m. This difference is due to a small deviation of the effective isotropic radiation power (EIRP) of the horn antenna in both models which in the case of the simulated model, it was set from the input power excitation at the feeding port of the antenna which was calculated taking into account the calibrated antenna Gain (5.1 dB), the insertion losses of the feeding table (4.1 dB), the impedance mismatch of the antenna because of the proximity of the phantom ($|S_{11}| = 0.7$), and the maximum transmission power of the generator (30 dBm). Therefore, the EIRP of the antenna was set as 22.97 dBm in the simulation model. Local SAR calculation was done through the equation in (2) considering the mass density $\rho = 1000$ kg/m^3, the measured conductivity of the tissue-equivalent liquid at 850 MHz, $\sigma_{TEL} = 0.928$ S/m and the Electric field which was measured with a sampling interval of 500 ms and an averaging duration of 250 ms. The 2D RMSE between measured and simulated SAR patterns is 1.06 mW/kg.

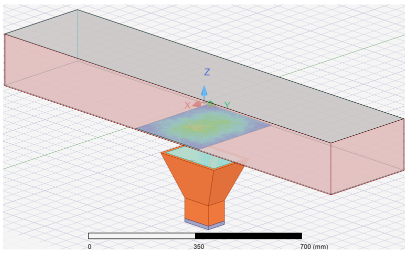

Fig. 4. Simulation model of the validation test

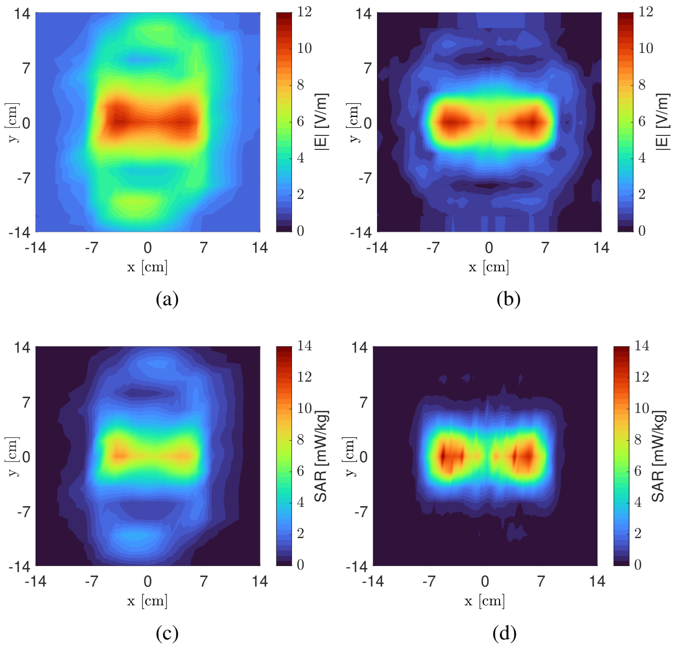

Fig. 5. 2D hot maps obtained from experimental measurements and simulation model **a)** Measured E-Field. **b)** Simulated E-Field. **c)** Measured SAR. **d)** Simulated SAR.

IV. Conclusion

We have presented a validated experimental setup for Electric field and SAR measurements in a flat human phantom model. Different test were proposed to illustrate the main specifications of the system. An optical tracking system was integrated reaching an accuracy of less than 1 mm and a precision of less than 0.02 mm which allows to associate the tracked position of the E-field probe with the measured electric field. 2D hot maps were generated in the post-processing unit where a validation through simulation was implemented by proposing a radiation test with a double ridge horn antenna where results are in good agreement.

Acknowledgment

This work was funded by the Pontificia Universidad Javeriana through the project ID 9236.

References

[1] I. C. on Non-ionizing Radiation Protection (ICNIRP), "Guidelines for limiting exposure to electromagnetic fields (100 khz to 300 ghz)," *Health Phys*, vol. 118, no. 5, pp. 483–524, 2020.

[2] T. Teixeira and S. F. Hasan, "Assessing electromagnetic radiation in our environment," *IEEE Potentials*, vol. 35, no. 2, pp. 22–25, 2016.

[3] I. A. for Research on Cancer (IARC), "Iarc classifies radiofrequency electromagnetic fields as possibly carcinogenic to humans," *Press Release*, vol. 208, pp. 1–6, 2011.

[4] ——, "Non-ionizing radiation part 2: Radiofrequency electromagnetic fields," *IARC Monographs on the Evaluation of Cercinogenic Risks to Humans*, vol. 102, pp. 1–481, 2013.

[5] B. Beard, W. Kainz, T. Onishi, T. Iyama, S. Watanabe, O. Fujiwara, J. Wang, G. Bit-Babik, A. Faraone, J. Wiart, A. Christ, N. Kuster, A.-K. Lee, H. Kroeze, M. Siegbahn, J. Keshvari, H. Abrishamkar, W. Simon, D. Manteuffel, and N. Nikoloski, "Comparisons of computed mobile phone induced sar in the sam phantom to that in anatomically correct models of the human head," *IEEE Transactions on Electromagnetic Compatibility*, vol. 48, no. 2, pp. 397–407, 2006.

[6] Y. Okano, K. Ito, I. Ida, and M. Takahashi, "The sar evaluation method by a combination of thermographic experiments and biological tissue-equivalent phantoms," *IEEE Transactions on Microwave Theory and Techniques*, vol. 48, no. 11, pp. 2094–2103, 2000.

[7] K. Wake, T. Arima, S. Watanabe, and M. Taki, "Sar distributions in a child head phantom in the vicinity of recent mobile phones," in *2011 XXXth URSI General Assembly and Scientific Symposium*, 2011, pp. 1–4.

[8] "IEEE Recommended Practice for Determining the Peak Spatial-Average Specific Absorption Rate (SAR) in the Human Head from Wireless Communications Devices: Measurement Techniques," *IEEE Std 1528-2013 (Revision of IEEE Std 1528-2003)*, pp. 1–246, 2013.

[9] I. M. S. M. M. T. M. V. N. W. K. W. J. Cardis, E. Deltour, "Distribution of rf energy emitted by mobile phones in anatomical structures of the brain." *Phys Med Biol*, vol. 53, no. 11, pp. 2771–2783, 2008.

[10] A. Gallego, E. Pineda, M. Pérez, F. Román, and J. Araque, "Low-cost system for electromagnetic sar evaluation in a human phantom," in *2022 IEEE USNC-URSI Radio Science Meeting (Joint with AP-S Symposium)*, 2022, pp. 23–24.

[11] S. Rodríguez, A. Gallego, E. Pineda, J. Vargas, M. Perez, F. Román, and J. Araque, "Low-cost setup for electromagnetic sar evaluation in a human phantom," in *2022 16th European Conference on Antennas and Propagation (EuCAP)*, 2022, pp. 1–5.

[12] J. Duque, J. Arévalo, M. Patiño, J. Vargas, M. Pérez, F. Román, and J. Araque, "Multi-physics analysis of human exposition to electromagnetic fields by 5g systems," in *2022 IEEE USNC-URSI Radio Science Meeting (Joint with AP-S Symposium)*, 2022, pp. 27–28.

[13] "IEC/IEEE International Standard - Measurement procedure for the assessment of specific absorption rate of human exposure to radio frequency fields from hand-held and body-mounted wireless communication devices – Part 1528: Human models, instrumentation, and procedures (Frequency range of 4 MHz to 10 GHz)," *IEC/IEEE 62209-1528:2020*, pp. 1–284, 2020.

[14] "Determination of RF field strength, power density and SAR in the vicinity of base stations for the purpose of evaluating human exposure," *IEC 62232:2022 (Revision of IEC 62232:2017)*, pp. 1–284, 2022.

[15] Anritsu. (2022) Vna master ms2027c. [Online]. Available: https://www.anritsu.com/en-gb/test-measurement/products/ms2027c

[16] Speag. (2022) Dak – dielectric assessment kit product line. [Online]. Available: https://speag.swiss/products/dak/overview/

[17] R. . SCHWARZ, *R&S®SMW200A VECTOR SIGNAL GENERATOR Specifications*, ROHDE & SCHWARZ, jan 2022.

[18] I. A.H. Systems, *SAS-571 Double Ridge Guide Horn Antenna*, A.H. Systems, Inc., 2022.

[19] Speag. (2022) Bstp-a - base station phantom adult. [Online]. Available: https://speag.swiss/components/phantoms/phantoms-3/base-station-phantom-a-2/

[20] ——. (2022) Head tissue simulating liquids. [Online]. Available: https://speag.swiss/components/materials-liquids/hsl/

[21] ——. (2022) Ef3dv3 isotropic e-field probe for general near-field measurements. [Online]. Available: https://speag.swiss/components/probes-2/e-field/ef3d-2/